

OSKDet: Towards Orientation-sensitive Keypoint Localization for Rotated Object Detection

Dongchen Lu

Abstract

Rotated object detection is a challenging issue of computer vision field. Loss of spatial information and confusion of parametric order have been the bottleneck for rotated detection accuracy. In this paper, we propose an orientation-sensitive keypoint based rotated detector OSKDet. We adopt a set of keypoints to characterize the target and predict the keypoint heatmap on ROI to form a rotated target. By proposing the orientation-sensitive heatmap, OSKDet could learn the shape and direction of rotated target implicitly and has stronger modeling capabilities for target representation, which improves the localization accuracy and acquires high quality detection results. To extract highly effective features at border areas, we design a rotation-aware deformable convolution module. Furthermore, we explore a new keypoint reorder algorithm and feature fusion module based on the angle distribution to eliminate the confusion of keypoint order. Experimental results on several public benchmarks show the state-of-the-art performance of OSKDet. Specifically, we achieve an AP of 77.81% on DOTA, 89.91% on HRSC2016, and 97.18% on UCAS-AOD, respectively.

1. Introduction

With the success of deep convolutional neural networks (CNN), object detection has made an unprecedented breakthrough in recent years. General detection models [11, 16, 31] regress the horizontal bounding box of objects. However, real scenes targets may have arbitrary directions, such as cars in drone cameras and texts in streetscape. Only determining the horizontal box is not enough to locate the target accurately. Rotated object detection has a wide range of applications, but still faces great challenges.

Recently, CNN based rotated detection has made a considerable progress. Some works [3, 6, 28, 42, 45] use the angle definition (coordinates of the central point, width, height, and rotated angle) to represent the rotated target. Other works [21, 25, 30, 38, 46] use vertex definition (coordinates of four vertices) to describe the rotated quadrilateral. Mainstream models mainly face the following issues:

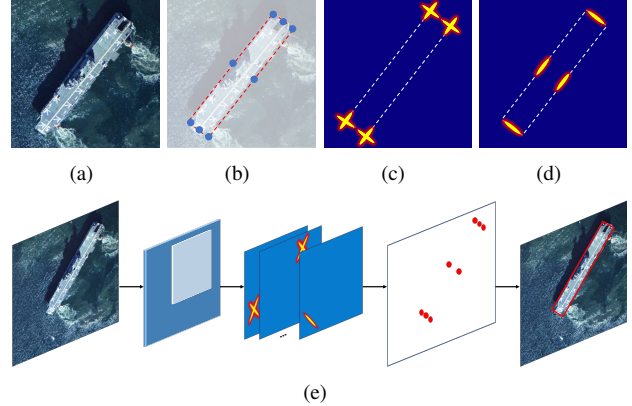


Figure 1. (a) a rotated target represented by 8 keypoints in (b). (c) and (d) display the proposed orientation-sensitive heatmap, we encode the keypoint to cross-star shape in corner and straight shape in edge areas, which represents the outline of target more accurately. (e) OSKDet: keypoint based detector. OSKDet generates the orientation-sensitive keypoint heatmap through fully convolution structure, which has a strong modeling ability of spatial representation and achieves high quality detections.

i) loss of spatial information, as traditional regression based detection models utilize spatial information insufficiently, and will lose this relative location information. For rotated targets with more random positions and directions, the missing of spatial information weakens the capability of localization; ii) confusion of parametric order, which is caused by the parametric exchangeability and definition periodicity of rotated targets, and manual labeling errors exacerbate this problem. Similar samples with different optimization direction will cause learning confusion. In fact, these issues can largely affect the detection performance especially at the localization accuracy.

In this paper, we propose a keypoint based rotated detector OSKDet. We encode a set of keypoints to represent rotated target. To avoid the loss of spatial information, we drop the fully connected layer and adopt the fully convolution block to generate keypoint heatmap on ROI. Considering that rotated target has more obvious features at the vertex and edge areas, we design an orientation-sensitive heatmap, as shown in Fig 1(c) and Fig 1(d), which could

better match the target shape, and the network could learn the orientation and shape of rotated target implicitly. OSKDet has stronger modeling capabilities in spatial representation and transformation. Furthermore, we propose a rotation-aware deformable convolution module to extract the target border feature more effectively. We also explore a keypoint reorder algorithm based on the dataset angle distribution, which could eliminate the keypoint order confusion problem to the greatest extent.

The proposed three modules can notably improve rotated detection accuracy. Extensive experiments on public benchmarks, including aerial dataset DOTA[37], HRSC2016[26], UCAS-AOD[50], scene text dataset ICDAR2015[15] and ICDAR2017MLT[29], show the superiority of OSKDet.

Our main contributions can be summarized as follows:

1) We propose a keypoint based rotated detector OSKDet that predicts the keypoint heatmap on the ROI. We design an orientation-sensitive heatmap, which could learn the shape and direction of rotated target, and plays a significant role in improving the localization accuracy.

2) We propose a rotation-aware deformable convolution module, which could extract the features of target border regions more effectively.

3) We explore a new angle distribution based keypoint reorder algorithm to eliminate keypoint order confusion. And on this basis, a new local and global feature fusion module is proposed.

2. Related work

2.1. Horizontal object detection

Detection models with deep neural networks achieved superior performance on the public datasets COCO[20] and VOC[9] recently. According to whether there is a series of candidate anchor box, detection models can be divided into anchor based and anchor free methods. While according to the final localization mode, existing models have regression and heatmap methods. Most anchor based detectors localize targets by regression mode. Faster RCNN[34], FPN[19], Cascade RCNN[2] etc. use fully connected layers to predict the deviation between anchor box and target. YOLO v2[32] and YOLO v3[33] adopt fully convolution structure and regress target center point ratio on each grid cell. Recently some anchor free methods detect targets mainly by generating heatmap of keypoints. CenterNet[8], CornerNet[16], ExtremeNet[49] etc. predict the probability of center or corner point in the whole image, and then group the points to form a box. Grid RCNN[27] predicts the keypoint heatmap on ROI and acquires a higher localization accuracy compared to Faster RCNN[34].

2.2. Rotated object detection

Similar to the horizontal object detection, mainstream rotated detection algorithms can be divided into anchor based and anchor free models, in which anchor based models have horizontal and rotated anchor box. According to the definition of rotated target, there are two types of prediction mode: angle representation and vertex representation. Angle definition uses the rotated angle(θ) of the longer border around the horizontal axis as the fifth parameter, with other parameters constitute the expression paradigm of rotated target (x, y, w, h, θ) . Vertex representation indicates rotated target by marking four vertices of the quadrilateral $(x_0, y_0, x_1, y_1, x_2, y_2, x_3, y_3)$. Compared to angle notation, vertex notation can represent any shape quadrilateral, and as mentioned in [30], the four vertices regression has natural consistency, which means it is easier to optimize.

Angle based detector. DRBox[23] and R2PN[45] introduce rotated anchor box based on rotated RPN. RRPN[28] proposes rotated ROI pooling to extract feature more effectively. R2CNN[14] regresses two adjacent vertices and another side length of rotated target. ROI transformer[6] transforms horizontal proposals to rotated ones through fully connection learning in RPN stage. EAST[48] regresses the distance between each pixel and four sides of rotated box. SCRDet[42] highlights the target features through attention module, and proposes IOU smooth L1 loss to smooth the boundary loss jump. CSL[40] transforms angle prediction from regression to classification, and proposes circular label smooth. PIOUS[3] adopts pixel counting method to calculate polygon IOU and makes it approximately derivable.

Vertex based detector. Textboxes++[18] proposes irregular long convolution kernel to adapt to targets with large aspect ratio. Gliding Vertex[38] regresses the ratio of the four vertices relative to the four points of horizontal box, and proposes an obliquity factor distinguishing nearly horizontal and other rotated objects. PolarDet[46] adopts several vertices angles and length ratio around the center point in polar coordinates to generate rotated box. SBD[25] proposes sequential-free box discretization parameterizing rotated boxes into key edges to eliminate the sensitive of label sequence. RSDet[30] proposes modulated loss by swapping point set sequence to obtain the best optimization direction.

3. Proposed methods

Overview. In this section, we first present two main issues that hinder the rotated detection accuracy, and then introduce our method.

Loss of spatial information. Mainstream rotated detector adopt fully connected layers and regression method to localize target. As [47] proposed the flattening operation of fully connected layers will lose spatial context information. While the convolution module has the ability to locate

target and maintain these relative information, and there is a pixel mapping relationship between the image and feature map. Compared to horizontal detection, rotated target has more complex spatial location diversity and transform feature, especially in the border regions. The spatial information plays a considerable role in localization accuracy.

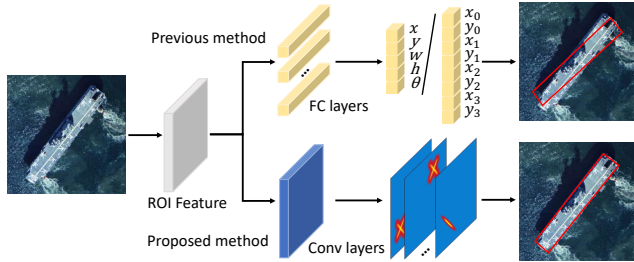


Figure 2. Previous method: previous works regress rotated angle or coordinates of vertex through fully connected layers. Proposed method: OSKDet predicts the keypoint by generating heatmap through full convolution block, which can preserve the spatial information loss and has stronger spatial generalization ability.

Confusion of parametric order. Both two definition methods have learning confusion problems, especially in the definition boundaries. For the angle representation, as shown in Fig 3(c), when the target is near a standard square, a little borderline length variety may lead to the exchange of width and height, and there is a $\pi/2$ jump in angle. Similar phenomena appear in the vertex representation, as illustrated in Fig 3(d), a slight spin may cause the vertex order transform. In the training process, two similar samples with quite different labels will lead to completely different optimization directions.

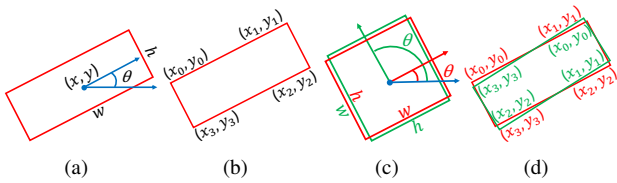


Figure 3. Different rotation representation: (a) angle notation. (b) vertex notation. (c) and (d) show parameters confusion. In (c), the red and green targets are very similar, while different length sequence causes width and height exchange, and their angle has $\pi/2$ gap. In (d), the red and green target has a slight rotation deviation, which leads to the vertex order one bit clockwise move.

The proposed method is based on the horizontal anchor box. Inspired by Grid RCNN[27], we predict the keypoint heatmap on horizontal ROI. Specifically, we adopt four vertices and four edge midpoints to represent a complete rotated target. The network architecture is shown in Fig 5. After deep feature extraction and RPN filtering, we feed the multi-path fused ROI feature into the keypoint head, and get fine-grained keypoint heatmap through twice decon-

volution. We design a new orientation-sensitive heatmap and a rotation-aware deformable convolution module. OSKDet has two optional branch outputs. Through the red branch, OSKDet outputs the orientation-sensitive heatmap. Through the blue branch, the network can obtain more accurate localization through the rotation-aware deformable convolution. Furthermore, we explore a minimum confusion keypoint reorder method as a preprocess module in the training stage. We will introduce each module in detail next.

3.1. Orientation-sensitive heatmap

[12, 16, 27] propose different heatmap generation methods. Gaussian distribution heatmap adopted by[8, 16, 49] is most widely used. Different encoding methods affect the final detection accuracy. In this section, we propose a novel orientation-sensitive heatmap (OSH), which is different from previous work. Next, we will introduce the generation mode of the new heatmap and the comparison with the standard gaussian heatmap (SGH).

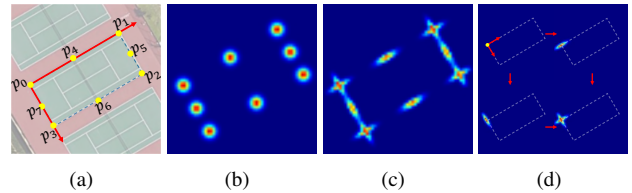


Figure 4. (a) a set of 8 ordered points representing a rotated target, including 4 vertices p_{0-3} and 4 midpoints p_{4-7} . (b) and (c) are the comparison of SGH and proposed OSH. Compared to the SGH with same variance in x and y axis, the OSH assigns different weights according to the importance of the area, which more accurately reflects the contours of vertex and edge. (d) displays the generation of OSH for the vertex p_0 .

For the p_0 point in Fig 4(a), compared with other regions, the intersection area of p_0p_1 and p_0p_3 have more obvious color and texture transformation, and the edge between two vertices has similar feature. We believe that the junction zone information is more important, and hope that the network output has higher response values in these areas. The proposed OSH encodes different response values according to the importance of spatial region. In Fig 4(a), we establish new coordinate axis in the direction of p_0p_1 and p_0p_3 respectively, in which direction the gaussian distribution has greater variance, as shown in Fig 4(c). OSH has stronger spatial representation and transformation ability.

After getting the proposal ROI from RPN, we map the ground truth keypoints to the ROI space. In order to include as many keypoints as possible, we adopt the ROI expansion idea of Grid RCNN[27], and expand the ROI from the center to $(1 + r)$ times size (r is set to 0.25). Assuming that the original ROI region is (x, y, w, h) , where (x, y) is the left-top point of the ROI, we obtain the expanded ROI (x', y', w', h') through Eq 1.

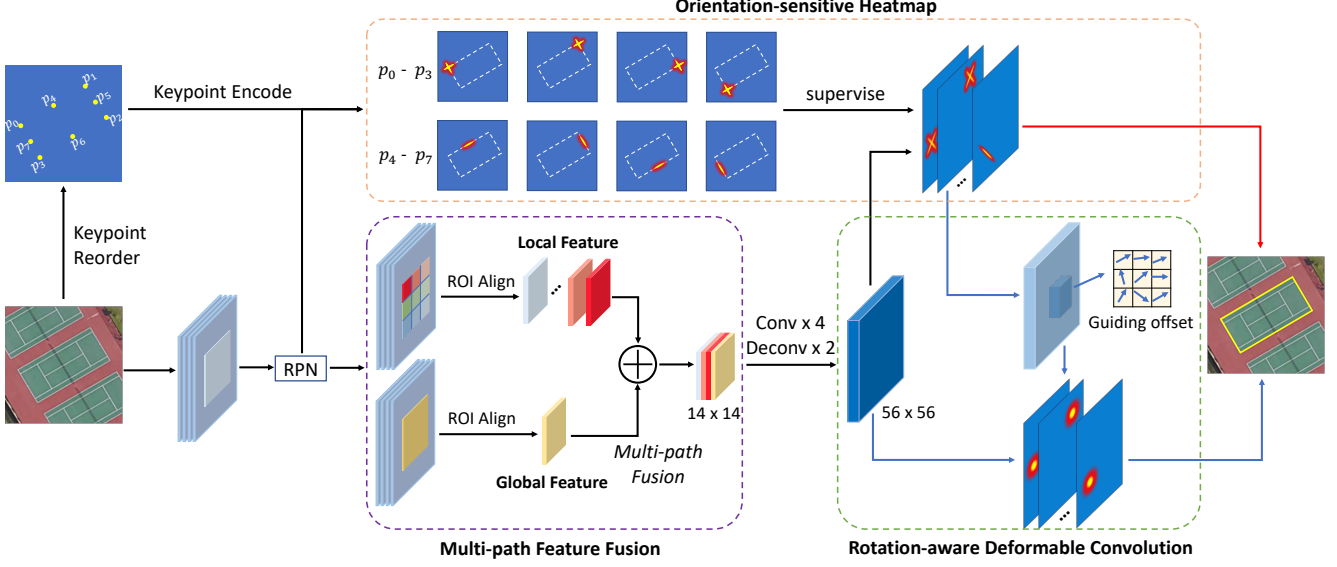


Figure 5. Architecture of the proposed OSKDet. OSKDet contains a keypoint reorder preprocess module (KR), a multi-path feature fusion module (MFF), an orientation-sensitive heatmap modeling (OSH) and a rotation-aware deformable convolution module (RCN). OSKDet has two optional output branches. After the MFF fusion, the red branch generates the OSH format heatmap, by which we get the keypoint representation of the target spatial modeling. The blue branch take the OSH as the RCN coordinate offset learning input, and get a more accurate localization through RCN. We get final detections after decoding either heatmap.

$$\begin{aligned} x' &= x - \frac{r}{2}w, & y' &= y - \frac{r}{2}h \\ w' &= (1+r)w, & h' &= (1+r)h \end{aligned} \quad (1)$$

Define the ground truth keypoints $P = \{p_k\}_{k \in [0, K-1]}$, $p_k = (\hat{x}_k, \hat{y}_k)$ and mapped keypoints $Q = \{q_k\}_{k \in [0, K-1]}$, $q_k = (x_k, y_k, \theta_k)$. we adopt a total of $K = 8$ keypoints. After twice deconvolution, We will get a heatmap of $M \times M$ size (default $M = 56$). Through Eq 2, we calculate the mapped coordinates on the heatmap. For the mapped points beyond ROI boundary, the generated heatmap is all 0.

$$x_k = (\hat{x}_k - x') \frac{M}{w'}, \quad y_k = (\hat{y}_k - y') \frac{M}{h'} \quad (2)$$

For the vertex q_{0-3} , we calculate the rotated angle θ in the direction of two adjacent sides (e.g. for q_0 , we calculate the angle of q_0q_1 and q_0q_3 directions).

$$\theta_k = \left[\arctan \left(\frac{y_{(k+1)\%4} - y_k}{x_{(k+1)\%4} - x_k} \right), \arctan \left(\frac{y_{(k-1)\%4} - y_k}{x_{(k-1)\%4} - x_k} \right) \right] \quad (3)$$

For the midpoint q_{4-7} , we only calculate the rotated angle formed by the vertices on both sides (e.g. for q_4 , we calculate the angle of q_0q_1 direction).

$$\theta_k = \arctan \left(\frac{y_{(k-3)\%4} - y_{k-4}}{x_{(k-3)\%4} - x_{k-4}} \right) \quad (4)$$

Suppose the mean and covariance matrix of standard gaussian distribution be $\mu_k = (x_k, y_k)^T$, $\Sigma = \begin{bmatrix} \sigma_{11} & 0 \\ 0 & \sigma_{22} \end{bmatrix}$. The rotation matrix of cartesian coordinate

about the origin is $R_k = \begin{bmatrix} \cos \theta_k & -\sin \theta_k \\ \sin \theta_k & \cos \theta_k \end{bmatrix}$. The covariance matrix after rotation transformation is

$$\Sigma_k = R_k^T \Sigma R_k \quad (5)$$

The final OSH is generated by Eq 6. For the vertex q_{0-3} , we generate heatmap in two directions. Fig 4(d) displays the OSH generation process.

$$H(g)_k = \frac{1}{\sqrt{2\pi|\Sigma_k|}} \exp \left[-\frac{1}{2} (g - \mu_k)^T \Sigma_k^{-1} (g - \mu_k) \right] \quad (6)$$

We adopt the binary cross entropy loss function to optimize the regression error of the heatmap, as illustrated by Eq 7. The $\delta(\cdot)$ is sigmoid function.

$$\begin{aligned} Loss &= \frac{1}{K \times M \times M} \sum_{k=0}^{K-1} \sum_{i=0}^{M-1} \sum_{j=0}^{M-1} - \left(h_{kij} \right) \log \left(\delta \left(h_{kij} \right) \right) \\ &\quad - \left(1 - h_{kij} \right) \log \left(1 - \delta \left(h_{kij} \right) \right) \end{aligned} \quad (7)$$

3.2. Rotation-aware deformable convolution

The vertex and edge regions of rotated target have more valuable features. We hope that the model can capture more effective features at these important areas to form a kind of spatial attention, which needs the convolution kernel to have the feature extraction capabilities for irregular shapes. Inspired by deformable convolution[4] and cross-star deformable convolution[7], we propose a new rotation-aware

convolution (RCN), as shown in Fig 6. The orientation-sensitive heatmap in previous section acts as an ‘‘attention module’’ to guide the generation of coordinate offset. The OSH accurately represents rotated target in the vertex and edge regions. By learning the geometric structure of OSH, the network will be more attentive to these valuable areas.

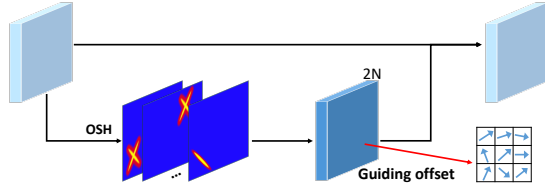


Figure 6. Rotation-aware deformable convolution module: RCN takes OSH format heatmap as coordinate offset learning input, and generates more accurate sampling points for feature extraction.

Different from DCN with fully autonomous learning, RCN take the supervised OSH as offset learning guidance. The OSH contains both shape and direction information, which could be transformed into sampling coordinate offset through the guided learning. Fig 7 depicts the receptive field of different CNN modules. Compared with CNN and DCN, the sampling points of RCN are more consistent with the contour of the object, by which we could extract more valuable features. Experimental results prove that RCN will further improve localization precision.

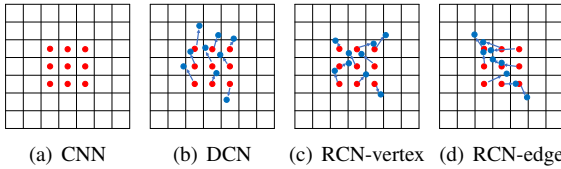


Figure 7. Receptive field of different convolution methods: Compared with CNN and DCN, RCN can learn the shape and direction guided offset from the OSH. In the vertex region, the convolution has a rotated cross-star shape sampling points in (c). In the middle of edge area, the reception field shape is inclined straight in (d).

3.3. Keypoint reorder

The root of keypoint order confusion lies in the point order transform on the keypoint sorting interface. Most works adopt an angle to sort keypoint, e.g. in Gliding Vertex[38], the author defines the vertex with smallest ordinate as the first point, and then clockwise ordering, which means they choose the horizontal 0° as the interface. The confusion near 0° is largest, as a slight angle spin will cause the point sets order transform, such as the two cars in Fig 8(a). And in any angle, there is such a confusion problem.

Our method is to minimize the confusion, that is, we need to find an angle value that contains as few instances as possible nearby. We study the angular distribution of the training set. We first find the vertex with the smallest ordinate (for horizontal rectangle, we take the top-left point)

as the first point v_i , then reorder it clockwise to find the last point $v_{(i-1)\%4}$, and calculate the angle between v_i and $v_{(i-1)\%4}$. Take DOTA[37] dataset as an example, the angle distribution is shown in the Fig 8(d).

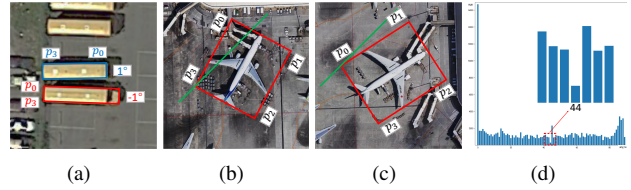


Figure 8. (a) Two similar samples with different labels in the 0° interface. (b) and (c) show two cases of our method to sort keypoint order, the green line is minimum angle interface, instance across this angle threshold will transform point order. (d) DOTA angle statistics, the instances size near 44° is the least.

For DOTA[37], the angle statistics in $44-45^\circ$ interval are the smallest, and the predicted error tolerance rate in this interval is relatively highest. The statistics near 0° (90°) is the largest, which means that the confusion here is also the largest. We reorder 4 vertices according to the minimum confusion angle by Algorithm 1, and then 4 midpoints. Fig 8(b) and Fig 8(c) display two cases of our keypoint sorting algorithm.

Algorithm 1 Keypoint Reorder

Input: 4 vertices (v_0, v_1, v_2, v_3)

Output: 4 ordered keypoints (p_0, p_1, p_2, p_3)

- 1: $V \leftarrow \{v_0, v_1, v_2, v_3\}$;
 - 2: $i = \text{find the index of top point}(V)$;
 - 3: **if** $y_i = y_{(i-1)\%4}$ **then**
 - 4: $i \leftarrow (i - 1)\%4$;
 - 5: $\text{angle} = \text{arctan} \left(\frac{y_i - y_{(i-1)\%4}}{x_i - x_{(i-1)\%4}} \right)$;
 - 6: **if** $\text{angle} > \text{threshold}$ **then**
 - 7: **return** $v_i, v_{(i+1)\%4}, v_{(i+2)\%4}, v_{(i+3)\%4}$;
 - 8: **else**
 - 9: **return** $v_{(i+1)\%4}, v_{(i+2)\%4}, v_{(i+3)\%4}, v_i$;
-

Each point after reordering has a relatively fixed position, which could provide a more accurate location information. We design a multi-path feature fusion module (MFF). By superimposing global feature and more precise local features on different channels, MFF could utilize the location information more effectively, as shown in Fig 9. In detail, we split the ROI area to $N \times N$ grids (N is set to 3) and define the local feature as $L(i, j), i, j \in [1, N]$. MFF extracts the global and local feature by ROI Align at the same time, and fuse them according to the point rough location. For DOTA, when we choose 44° as the keypoint reorder interface, the first keypoint p_0 can only occur in the left-top triangle region of the ROI, and the local area is $(1,1), (1,2), (1,3), (2,1), (2,2)$ and $(3,1)$, and so are other keypoints, as the color labeled grids in the ROI of Fig 9 right side depicts. The k th

keypoint feature fusion can be defined by Eq 8. When one grid cell falls into the region where the point is located, the coefficient c_k of this grid is 1, otherwise 0.

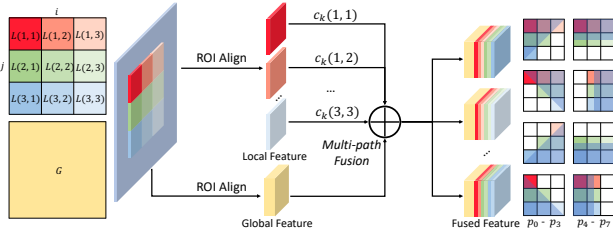


Figure 9. Multi-path feature fusion. Each point has a relatively fixed region, as the colored grids in the box on the right side. We fuse global and local features according to the point location.

$$F_k = \sum_{i=1}^3 \sum_{j=1}^3 c_k(i,j) * L(i,j) + G \quad (8)$$

4. Experiments

4.1. Dataset and implementation details

To compare the performance of OSKDet with the state-of-the-art methods, we conduct evaluations on several public datasets, including aerial detection dataset DOTA[37], HRSC2016[26] and UCAS-AOD[50], text detection dataset ICDAR2015[15] and ICDAR2017MLT[29].

DOTA[37] contains 2806 aerial images, ranging in size from $800 * 800$ to $4000 * 4000$, and contains 188282 instances in 15 categories. Train, validation and test set are split to 3:1:2. Same as other models, we use train set and validation set for training. We adopt the same processing strategy as [6, 38], which cropped the image to $1024 * 1024$ with 824 pixels as a stride.

HRSC2016[26] is a high resolution ship recognition dataset which contains 1061 images, and the image size ranges from $300 * 300$ to $1500 * 900$.

UCAS-AOD[50] contains 1510 aerial images of about $659 * 1280$ pixels, with 2 categories (car and plane) of 14,596 instances.

ICDAR2015[15] and **ICDAR2017MLT**[29] are two incidental scene Text dataset. Both of them contain natural scene text images with location annotations. IC15 has 1500 images and IC17 has 18000 images.

OSKDet is implemented on pytorch. We use 3 RTX 2080ti GPU, 2 images per GPU in our experiment. We adopt the FPN[19] based ResNet50[13] and ResNet101 as our backbone. We train 12 epochs in total by using momentum gradient descent optimization. The weight decay is set to 0.0001 and momentum is set to 0.9. The initial learning rate was 0.0075 and divided by 10 at (8, 11) epochs. For aerial set, we resize the image to $1 \times$ and $0.5 \times$ scales and use random rotation (0° , 90° , 270°) in training. For text set, we resize the longer side to {800, 1000, 1200}. We also adopt class balancing for DOTA.

4.2. Aerial detection

DOTA. Tab 3 shows our testing results on the DOTA v1.0 OBB task. Compared with the state-of-the-art methods, OSKDet shows superior performance. With ResNet50 as backbone, OSKDet achieves 76.22% AP, which excels most models with deeper feature extractor. With ResNet101 as backbone, OSKDet achieves 77.81% AP, which outperforms all previous works. Compared with the angle based detectors[28, 40, 41], OSKDet improves the state-of-the-art method by 1.00% AP. Compared with other vertex based detectors[46, 38, 30], OSKDet improves the state-of-the-art method by 1.17% AP. Compared with the vertex offset regression method[38], OSKDet improves AP by 2.79%. Furthermore, OSKDet has achieved the best performance in multiple categories, especially in irregularly shaped categories such as baseball diamond, ship and helicopter, which illustrates the great advantages of OSKDet in spatial representation and transformation. Through accurate characterization and feature extraction of keypoints, OSKDet is more effective in detecting complex and irregular shape targets.

HRSC2016 and UCAS-AOD. Tab 1 depicts the comparison of different methods on HRSC2016[26] and UCAS-AOD[50]. OSKDet achieves 89.91% AP and 97.18% AP respectively in the two challenging datasets and outperforms all other methods, which demonstrates the proposed OSKDet brings consistent gain on different aerial datasets.

Method	AP	Method	Plane	Car	AP
RoI-Trans[6]	86.20	S2ARN[1]	97.60	92.20	94.90
RSDet[30]	86.50	FADet[17]	98.69	92.72	95.71
Gliding Vertex[38]	88.20	R3Det[39]	98.20	94.14	96.17
BBAVectors[44]	88.60	SCRDet++[41]	98.93	94.97	96.95
CSL[40]	89.62	PolarDet[46]	99.08	94.96	97.02
OSKDet(ours)	89.91	OSKDet(ours)	99.07	95.29	97.18

Table 1. Comparison with state-of-the-art methods on HRSC2016 (left) and UCAS-AOD (right).

Ablation study. We perform all ablation experiments on DOTA dataset. Unless otherwise specified, all test benchmarks are VOC2007[9] AP.5 IOU metric. Tab 2 shows the comprehensive ablation experiment results.

Method	MS	OSH	RCN	KR	MFF	AP.5	FPS
OSKDet	✓					73.38	-
	✓	✓				75.54	-
	✓	✓	✓			76.16	8.15
	✓	✓	✓			76.86	7.91
	✓			✓		76.10	-
	✓			✓	✓	76.75	6.88
	✓	✓		✓		76.66	-
	✓	✓	✓	✓	✓	76.06	6.13
					77.81	-	

Table 2. Ablation experiment of different strategies on DOTA. MS, OSH, RCN, KR and MFF mean multi-scale training and testing, orientation-sensitive heatmap, rotation-aware deformable convolution, keypoint reorder and multi-path feature fusion respectively.

Orientation-sensitive heatmap. We compare the proposed method with different predicting formats, in-

Method	Backbone	PL	BD	BR	GTF	SV	LV	SH	TC	BC	ST	SBF	RA	HA	SP	HC	AP.5
FR-O[37]	ResNet101	79.09	69.12	17.17	63.49	34.20	37.16	36.20	89.19	69.6	58.96	49.40	52.52	46.69	44.80	46.30	52.93
IENet[21]	ResNet101	80.20	64.54	39.82	32.07	49.71	65.01	52.58	81.45	44.66	78.51	46.54	56.73	64.40	64.24	36.75	57.14
PIOU[3]	DLA-34	80.90	69.70	24.10	60.20	38.30	64.40	64.80	90.90	77.20	70.40	46.50	37.10	57.10	61.90	64.00	60.50
R2CNN[14]	ResNet101	80.94	65.67	35.34	67.44	59.92	50.91	55.81	90.67	66.92	72.39	55.06	52.23	55.14	53.35	48.22	60.67
RRPN[28]	ResNet101	88.52	71.20	31.66	59.30	51.85	56.19	57.25	90.81	72.84	67.38	56.69	52.84	53.08	51.94	53.58	61.01
ROI-Trans[6]	ResNet101	88.64	78.52	43.44	75.92	68.81	73.68	83.59	90.74	77.27	81.46	58.39	53.54	62.83	58.93	47.67	69.56
RSDet[30]	ResNet152	90.10	82.00	53.80	68.50	70.20	78.70	73.60	91.20	87.10	84.70	64.30	68.20	66.10	69.30	63.70	74.10
Gliding Vertex[38]	ResNet101	89.64	85.00	52.26	77.34	73.01	73.14	86.82	90.74	79.02	86.81	59.55	70.91	72.94	70.86	57.32	75.02
FFA[10]	ResNet101	90.10	82.70	54.20	75.20	71.00	79.90	83.50	90.70	83.90	84.60	61.20	68.00	70.70	76.00	63.70	75.70
CenterMap[35]	ResNet101	89.83	84.41	54.60	70.25	77.66	78.32	87.19	90.66	84.89	85.27	56.46	69.23	74.13	71.56	66.06	76.03
CSL[40]	ResNet152	90.25	85.53	54.64	75.31	70.44	73.51	77.62	90.84	86.15	86.69	69.66	68.04	73.83	71.10	68.93	76.17
PolarDet[46]	ResNet101	89.65	87.07	48.14	70.97	78.53	80.34	87.45	90.76	85.63	86.87	61.64	70.32	71.92	73.09	67.15	76.64
SCRDet++[41]	ResNet101	90.05	84.39	55.44	73.99	77.54	71.11	86.05	90.67	87.32	87.08	69.62	68.90	73.74	71.29	65.08	76.81
OSKDet(Ours)	ResNet50	89.83	84.75	52.18	75.22	71.75	76.47	87.29	90.42	78.95	87.02	57.49	69.71	73.50	71.23	60.14	75.06
OSKDet-MS(Ours)	ResNet50	89.98	86.99	53.13	75.55	72.87	76.97	87.63	90.74	78.87	86.97	60.13	70.68	75.70	71.53	65.60	76.22
OSKDet(Ours)	ResNet101	89.88	86.26	53.42	74.40	72.23	76.80	87.34	90.81	78.98	86.39	57.97	71.59	75.60	72.20	67.07	76.06
OSKDet-MS(Ours)	ResNet101	90.04	87.25	54.41	79.48	72.66	80.29	88.20	90.84	83.91	86.90	63.39	71.76	75.63	72.59	69.75	77.81

Table 3. Comparison of different method results on DOTA-v1.0 OBB task (MS means multi-scale training and testing)

cluding vertex offset regression[38] (REG), single point heatmap[12] (SPH), cross-star heatmap[27] (CSH), standard gaussian heatmap[16] (SGH) and orientation-sensitive heatmap (OSH). We implement the four different format heatmaps on OSKDet. Tab 4 displays the result. The OSH surpasses all baselines with an increment of 0.62%-1.15%. Compared with the SGH, the OSH improves 0.68% and 0.62% AP without/ with FPN respectively, which proves the stronger spatial modeling capabilities of OSH will bring localization accuracy gains.

Method	FPN	AP.5
REG[38]		73.39
SGH[16]		73.86(+0.47)
OSH(Ours)		74.54(+1.15)
REG[38]	✓	75.02
SPH[12]	✓	75.11
CSH[27]	✓	75.42
SGH[16]	✓	75.54(+0.52)
OSH(Ours)	✓	76.16(+1.14)

Table 4. Comparison of different prediction format results

To further verify the effect of OSH and find best parameters, we try different gaussian kernel ratio and kernel size combination experiment. As shown in Fig 10, σ represents the standard deviation in the vertical direction σ_{22} , and r represents the scale factor between the axis direction and the vertical direction, that is, $\sigma_{11} = r * \sigma_{22}$ ($r = 1$ means SGH). We get the best effect when $r = 3$ and $\sigma = 0.8$.

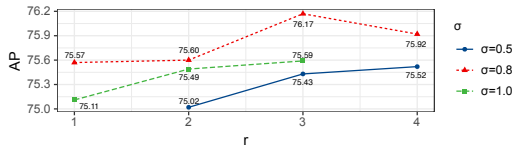


Figure 10. Comparison of different σ and r results on OSH. The two parameters represent the direction of rotated object. More accurate characterization will improve the localization accuracy, which demonstrates the superiority of OSH.

Since the DOTA[37] official evaluation system only provides the test results for AP.5 metric. In order to test the

performance of the model under different IOU metrics, we use the training set to train and validation set to evaluate. We reimplement [38] and other format heatmap in OSKDet. The OSH achieves 43.82% mAP, which excels other format predictions with considerable performance gains, specifically 3.04%, 2.69%, 2.00% and 1.06% mAP for REG, SPH, CSH and SGH. As illustrated in Fig 11, OSH surpasses all other method especially in the high IOU metric. Under AP.9 IOU threshold, OSH surpasses other methods by 2.33%-5.07%, which demonstrates that OSKDet has a huge advantage in obtaining high quality detections.

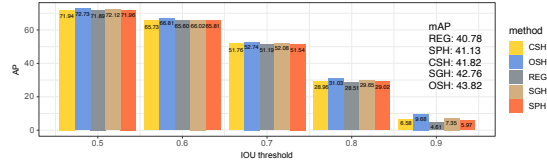


Figure 11. Comparison of different prediction format results under AP.5-.95 IOU metric on validation set

Rotation-aware deformable convolution. We compare the results of standard CNN, DCN, and RCN under AP.5-.95 metric. Same as the previous section, we use the training set to train and the validation set to test. The RCN improves the mAP by 1.27% and 0.75% respectively as shown in Tab 5. Through the guided learning of the OSH, RCN can extract highly effective features and obtain better localization results. As shown in Fig 13, when two targets are very close, standard CNN and DCN cannot distinguish them, while the more precise sampling points of RCN can accurately locate them respectively.

Method	DCN	RCN	AP.5	AP.75	AP.5-.95
OSKDet	✓	✓	72.09	42.98	42.86
			72.35	43.70	43.38(+0.52)
			72.84	44.52	44.13(+1.27)

Table 5. Comparison of different CNN module results under AP.5-.95 IOU metric on validation set

Keypoint reorder and multi-path feature fusion. We compare the original annotations (unsorted), 0° , 44° as the

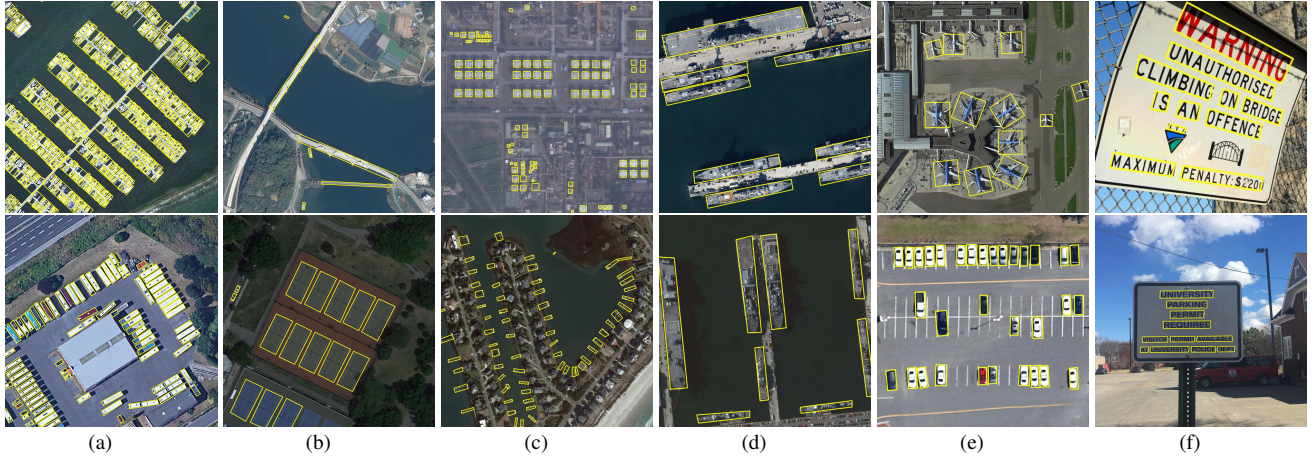


Figure 12. Visualization of OSKDet detections. (a)(b)(c): DOTA (d): HRSC2016 (e): UCAS-AOD (f): ICDAR

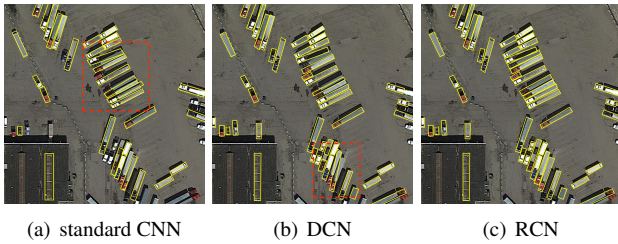


Figure 13. Different CNN modules detections. The red dashed box in (a)(b) is marked as false detection, where the network cannot accurately detect whether keypoints belong to the same target.

keypoint sorting interface, modulated loss[30] optimization method, 44° sorting and modulated loss (after training 2 epochs, use the modulated loss). Experiment results in Tab 6 show that our keypoint reorder method performs better than other methods, which improves AP by 0.99% compared to the baseline. We also study the precision of each angle interval in validation set. The precision near 44° is relatively low, but it maintains high accuracy in all other angle range, which proves the effectiveness of our algorithm for eliminating most of the samples confusion. The proposed feature fusion module also has a significant effect on localization precision by improving 0.65% AP, which further proves the significance of spatial information.

Method	KR-0	KR-44	MFF	ML	AP.5
OSKDet	✓				75.11
					75.49(+0.38)
		✓		✓	75.96(+0.85)
		✓	✓		76.10(+0.99)
		✓	✓	✓	76.75(+1.64)
					76.79(+1.68)

Table 6. Comparison of different keypoint sort methods. ML, KR-0, KR-44 and MFF mean modulated loss, 0° sorting interface, 44° sorting interface and multi-path feature fusion respectively.

4.3. Text detection

The text dataset has a greater challenge due to the large number of irregular quadrilaterals and large aspect ratio long text. Tab 7 shows our detection results on ICDAR2015[15] and ICDAR2017MLT[29]. OSKDet achieves 91.34% F-measure on IC15 and 80.29% F-measure on IC17, which are comparable to the state-of-the-art algorithms. Specifically, On IC15, OSKDet surpasses most of the state-of-the-art methods. Although there are still some gaps with [43], OSKDet does not need complex labeling and multi-task calculations in [43], which could avoid tedious preprocess and achieves a relatively fast inference speed. Our model could easily extend to other datasets. On IC17, without other techniques designed for text targets, OSKDet surpasses the state-of-the-art method by 0.18% F-measure, which proves the potential of OSKDet in OCR.

Task	Method	Recall	Precision	F-measure	FPS
ICDAR2015	EAST[48]	73.50	83.60	78.20	6.52
	PixelLink[5]	82.00	85.50	83.70	7.30
	PSENet[36]	85.22	89.30	87.21	2.33
	FOTS[24]	85.17	91.00	87.99	7.50
	Textfusetnet[43]	89.70	94.70	92.10	4.10
	OSKDet(ours)	88.35	94.56	91.34	6.31
ICDAR2017	PSENet[36]	68.35	76.97	72.40	-
	SBD[25]	70.10	83.60	76.30	-
	PMTD[22]	76.25	84.42	80.13	-
	OSKDet(ours)	75.69	85.53	80.31	6.01

Table 7. Comparison of different methods on ICDAR

5. Conclusion

This paper proposes a rotated object detection model OSKDet. By the proposed orientation-sensitive heatmap and rotation-aware deformable convolution, OSKDet can extract spatial feature effectively and obtain high quality detection results. The proposed keypoint sorting methods and feature fusion module eliminate the confusion of keypoint order greatly. Experimental results on several public datasets show the state-of-the-art performance of OSKDet.

References

- [1] Songze Bao, Xing Zhong, Ruifei Zhu, Xiaonan Zhang, Zhuqiang Li, and Mengyang Li. Single shot anchor refinement network for oriented object detection in optical remote sensing imagery. *IEEE Access*, 7:87150–87161, 2019.
- [2] Zhaowei Cai and Nuno Vasconcelos. Cascade r-cnn: Delving into high quality object detection. In *2018 IEEE/CVF Conference on Computer Vision and Pattern Recognition*, pages 6154–6162, 2018.
- [3] Zhiming Chen, Kean Chen, Weiyao Lin, John See, Hui Yu, Yan Ke, and Cong Yang. Piou loss: Towards accurate oriented object detection in complex environments. In *ECCV (5)*, pages 195–211, 2020.
- [4] Jifeng Dai, Haozhi Qi, Yuwen Xiong, Yi Li, Guodong Zhang, Han Hu, and Yichen Wei. Deformable convolutional networks. In *2017 IEEE International Conference on Computer Vision (ICCV)*, pages 764–773, 2017.
- [5] Dan Deng, Haifeng Liu, Xuelong Li, and Deng Cai. Pixellink: Detecting scene text via instance segmentation. In *AAAI*, pages 6773–6780, 2018.
- [6] Jian Ding, Nan Xue, Yang Long, Gui-Song Xia, and Qikai Lu. Learning roi transformer for oriented object detection in aerial images. In *2019 IEEE/CVF Conference on Computer Vision and Pattern Recognition (CVPR)*, pages 2849–2858, 2019.
- [7] Zhiwei Dong, Guoxuan Li, Yue Liao, Fei Wang, Pengju Ren, and Chen Qian. Centripetalnet: Pursuing high-quality keypoint pairs for object detection. In *2020 IEEE/CVF Conference on Computer Vision and Pattern Recognition (CVPR)*, pages 10519–10528, 2020.
- [8] Kaiwen Duan, Song Bai, Lingxi Xie, Honggang Qi, Qingming Huang, and Qi Tian. Centernet: Keypoint triplets for object detection. In *2019 IEEE/CVF International Conference on Computer Vision (ICCV)*, pages 6569–6578, 2019.
- [9] Mark Everingham, Luc Gool, Christopher K. Williams, John Winn, and Andrew Zisserman. The pascal visual object classes (voc) challenge. *International Journal of Computer Vision*, 88(2):303–338, 2010.
- [10] Kun Fu, Zhonghan Chang, Yue Zhang, Guangluan Xu, Keshu Zhang, and Xian Sun. Rotation-aware and multi-scale convolutional neural network for object detection in remote sensing images. *Isprs Journal of Photogrammetry and Remote Sensing*, 161:294–308, 2020.
- [11] Ross Girshick. Fast r-cnn. In *2015 IEEE International Conference on Computer Vision (ICCV)*, pages 1440–1448, 2015.
- [12] Kaiming He, Georgia Gkioxari, Piotr Dollar, and Ross Girshick. Mask r-cnn. *IEEE Transactions on Pattern Analysis and Machine Intelligence*, 42(2):386–397, 2020.
- [13] Kaiming He, Xiangyu Zhang, Shaoqing Ren, and Jian Sun. Deep residual learning for image recognition. In *2016 IEEE Conference on Computer Vision and Pattern Recognition (CVPR)*, pages 770–778, 2016.
- [14] Yingying Jiang, Xiangyu Zhu, Xiaobing Wang, Shuli Yang, Wei Li, Hua Wang, Pei Fu, and Zhenbo Luo. R 2 cnn: Rotational region cnn for arbitrarily-oriented scene text detection. In *2018 24th International Conference on Pattern Recognition (ICPR)*, pages 3610–3615, 2018.
- [15] Dimosthenis Karatzas, Lluís Gomez-Bigorda, Angelos Nicolaou, Suman Ghosh, Andrew Bagdanov, Masakazu Iwamura, Jiri Matas, Lukas Neumann, Vijay Ramaseshan Chandrasekhar, Shijian Lu, Faisal Shafait, Seiichi Uchida, and Ernest Valveny. Icdar 2015 competition on robust reading. In *2015 13th International Conference on Document Analysis and Recognition (ICDAR)*, pages 1156–1160, 2015.
- [16] Hei Law and Jia Deng. Cornernet: Detecting objects as paired keypoints. *International Journal of Computer Vision*, 128(3):642–656, 2020.
- [17] Chengzheng Li, Chunyan Xu, Zhen Cui, Dan Wang, Tong Zhang, and Jian Yang. Feature-attentioned object detection in remote sensing imagery. In *2019 IEEE International Conference on Image Processing (ICIP)*, pages 3886–3890, 2019.
- [18] Minghui Liao, Baoguang Shi, and Xiang Bai. Textboxes++: A single-shot oriented scene text detector. *IEEE Transactions on Image Processing*, 27(8):3676–3690, 2018.
- [19] Tsung-Yi Lin, Piotr Dollar, Ross Girshick, Kaiming He, Bharath Hariharan, and Serge Belongie. Feature pyramid networks for object detection. In *2017 IEEE Conference on Computer Vision and Pattern Recognition (CVPR)*, pages 936–944, 2017.
- [20] Tsung-Yi Lin, Michael Maire, Serge J. Belongie, James Hays, Pietro Perona, Deva Ramanan, Piotr Dollár, and C. Lawrence Zitnick. Microsoft coco: Common objects in context. In *European Conference on Computer Vision*, pages 740–755, 2014.
- [21] Youtian Lin, Pengming Feng, and Jian Guan. Ienet: Interacting embranchment one stage anchor free detector for orientation aerial object detection. *arXiv preprint arXiv:1912.00969*, 2019.
- [22] Jingchao Liu, Xuebo Liu, Jie Sheng, Ding Liang, Xin Li, and Qingjie Liu. Pyramid mask text detector. *arXiv preprint arXiv:1903.11800*, 2019.
- [23] Lei Liu, Zongxu Pan, and Bin Lei. Learning a rotation invariant detector with rotatable bounding box. *arXiv preprint arXiv:1711.09405*, 2017.
- [24] Xuebo Liu, Ding Liang, Shi Yan, Dagui Chen, Yu Qiao, and Junjie Yan. Fots: Fast oriented text spotting with a unified network. In *2018 IEEE/CVF Conference on Computer Vision and Pattern Recognition*, pages 5676–5685, 2018.
- [25] Yuliang Liu, Sheng Zhang, Lianwen Jin, Lele Xie, Yaqiang Wu, and Zhepeng Wang. Omnidirectional scene text detection with sequential-free box discretization. In *Proceedings of the Twenty-Eighth International Joint Conference on Artificial Intelligence*, pages 3052–3058, 2019.
- [26] Zikun Liu, Liu Yuan, Lubin Weng, and Yiping Yang. A high resolution optical satellite image dataset for ship recognition and some new baselines. In *6th International Conference on Pattern Recognition Applications and Methods*, pages 324–331, 2017.
- [27] Xin Lu, Buyu Li, Yuxin Yue, Quanquan Li, and Junjie Yan. Grid r-cnn. In *2019 IEEE/CVF Conference on Computer Vision and Pattern Recognition (CVPR)*, pages 7363–7372, 2019.

- [28] Jianqi Ma, Weiyuan Shao, Hao Ye, Li Wang, Hong Wang, Yingbin Zheng, and Xiangyang Xue. Arbitrary-oriented scene text detection via rotation proposals. *IEEE Transactions on Multimedia*, 20(11):3111–3122, 2018.
- [29] Nibal Nayef, Fei Yin, Imen Bizid, Hyunsoo Choi, Yuan Feng, Dimosthenis Karatzas, Zhenbo Luo, Umapada Pal, Christophe Rigaud, Joseph Chazalon, Wafa Khelif, Muhammad Muzzamil Luqman, Jean-Christophe Burie, Cheng lin Liu, and Jean-Marc Ogier. Icdar2017 robust reading challenge on multi-lingual scene text detection and script identification - rrc-mlt. In *2017 14th IAPR International Conference on Document Analysis and Recognition (ICDAR)*, pages 1454–1459, 2017.
- [30] Wen Qian, Xue Yang, Silong Peng, Yue Guo, and Chijun Yan. Learning modulated loss for rotated object detection. *arXiv preprint arXiv:1911.08299*, 2019.
- [31] Joseph Redmon, Santosh Divvala, Ross Girshick, and Ali Farhadi. You only look once: Unified, real-time object detection. In *2016 IEEE Conference on Computer Vision and Pattern Recognition (CVPR)*, pages 779–788, 2016.
- [32] Joseph Redmon and Ali Farhadi. Yolo9000: Better, faster, stronger. In *2017 IEEE Conference on Computer Vision and Pattern Recognition (CVPR)*, pages 6517–6525, 2017.
- [33] Joseph Redmon and Ali Farhadi. Yolo3: An incremental improvement. *arXiv preprint arXiv:1804.02767*, 2018.
- [34] Shaoqing Ren, Kaiming He, Ross Girshick, and Jian Sun. Faster r-cnn: Towards real-time object detection with region proposal networks. *IEEE Transactions on Pattern Analysis and Machine Intelligence*, 39(6):1137–1149, 2017.
- [35] Jinwang Wang, Wen Yang, Heng-Chao Li, Haijian Zhang, and Gui-Song Xia. Learning center probability map for detecting objects in aerial images. *IEEE Transactions on Geoscience and Remote Sensing*, pages 1–17, 2020.
- [36] Wenhai Wang, Enze Xie, Xiang Li, Wenbo Hou, Tong Lu, Gang Yu, and Shuai Shao. Shape robust text detection with progressive scale expansion network. In *2019 IEEE/CVF Conference on Computer Vision and Pattern Recognition (CVPR)*, pages 9336–9345, 2019.
- [37] Gui-Song Xia, Xiang Bai, Jian Ding, Zhen Zhu, Serge Belongie, Jiebo Luo, Mihai Datcu, Marcello Pelillo, and Liangpei Zhang. Dota: A large-scale dataset for object detection in aerial images. In *2018 IEEE/CVF Conference on Computer Vision and Pattern Recognition*, pages 3974–3983, 2018.
- [38] Yongchao Xu, Mingtao Fu, Qimeng Wang, Yukang Wang, Kai Chen, Gui-Song Xia, and Xiang Bai. Gliding vertex on the horizontal bounding box for multi-oriented object detection. *IEEE Transactions on Pattern Analysis and Machine Intelligence*, 2020.
- [39] Xue Yang, Qingqing Liu, Junchi Yan, and Ang Li. R3det: Refined single-stage detector with feature refinement for rotating object. *arXiv preprint arXiv:1908.05612*, 2019.
- [40] Xue Yang and Junchi Yan. Arbitrary-oriented object detection with circular smooth label. In *ECCV(8)*, pages 677–694, 2020.
- [41] Xue Yang, Junchi Yan, Xiaokang Yang, Jin Tang, Wenlong Liao, and Tao He. Scrdet++: Detecting small, cluttered and rotated objects via instance-level feature denoising and rotation loss smoothing. *arXiv preprint arXiv:2004.13316*, 2020.
- [42] Xue Yang, Jirui Yang, Junchi Yan, Yue Zhang, Tengfei Zhang, Zhi Guo, Xian Sun, and Kun Fu. Scrdet: Towards more robust detection for small, cluttered and rotated objects. In *2019 IEEE/CVF International Conference on Computer Vision (ICCV)*, pages 8232–8241, 2019.
- [43] Jian Ye, Zhe Chen, Juhua Liu, and Bo Du. Textfusenet: Scene text detection with richer fused features. In *Proceedings of the Twenty-Ninth International Joint Conference on Artificial Intelligence*, volume 1, pages 516–522, 2020.
- [44] Jingru Yi, Pengxiang Wu, Bo Liu, Qiaoying Huang, Hui Qu, and Dimitris N. Metaxas. Oriented object detection in aerial images with box boundary-aware vectors. *Proceedings of the IEEE/CVF Winter Conference on Applications of Computer Vision*, pages 2150–2159, 2020.
- [45] Zenghui Zhang, Weiwei Guo, Shengnan Zhu, and Wenxian Yu. Toward arbitrary-oriented ship detection with rotated region proposal and discrimination networks. *IEEE Geoscience and Remote Sensing Letters*, 15(11):1745–1749, 2018.
- [46] Pengbo Zhao, Zhenshen Qu, Yingjia Bu, Wenming Tan, Ye Ren, and Shiliang Pu. Polardet: A fast, more precise detector for rotated target in aerial images. *arXiv preprint arXiv:2010.08720*, 2020.
- [47] Bolei Zhou, Aditya Khosla, Agata Lapedriza, Aude Oliva, and Antonio Torralba. Learning deep features for discriminative localization. In *2016 IEEE Conference on Computer Vision and Pattern Recognition (CVPR)*, pages 2921–2929, 2016.
- [48] Xinyu Zhou, Cong Yao, He Wen, Yuzhi Wang, Shuchang Zhou, Weiran He, and Jiajun Liang. East: An efficient and accurate scene text detector. In *2017 IEEE Conference on Computer Vision and Pattern Recognition (CVPR)*, pages 2642–2651, 2017.
- [49] Xingyi Zhou, Jiacheng Zhuo, and Philipp Krahenbuhl. Bottom-up object detection by grouping extreme and center points. In *2019 IEEE/CVF Conference on Computer Vision and Pattern Recognition (CVPR)*, pages 850–859, 2019.
- [50] Haigang Zhu, Xiaogang Chen, Weiqun Dai, Kun Fu, Qixiang Ye, and Jianbin Jiao. Orientation robust object detection in aerial images using deep convolutional neural network. In *2015 IEEE International Conference on Image Processing (ICIP)*, pages 3735–3739, 2015.